



HAL
open science

Development, synthesis, and ^{68}Ga -Labeling of a Lipophilic complexing agent for atherosclerosis PET imaging

Jennyfer Yong-Sang, Fabienne Dioury, Vincent Meneyrol, Imade Ait-Arsa, Jean-Patrick Idoumbin, Florian Guibbal, Jessica Patche, Fanny Gimié, Ilya Khantalin, Joël Couprie, et al.

► To cite this version:

Jennyfer Yong-Sang, Fabienne Dioury, Vincent Meneyrol, Imade Ait-Arsa, Jean-Patrick Idoumbin, et al. Development, synthesis, and ^{68}Ga -Labeling of a Lipophilic complexing agent for atherosclerosis PET imaging. *European Journal of Medicinal Chemistry*, 2019, 176, pp.129-134. 10.1016/j.ejmech.2019.05.002 . hal-02500075

HAL Id: hal-02500075

<https://cnam.hal.science/hal-02500075>

Submitted on 22 Oct 2021

HAL is a multi-disciplinary open access archive for the deposit and dissemination of scientific research documents, whether they are published or not. The documents may come from teaching and research institutions in France or abroad, or from public or private research centers.

L'archive ouverte pluridisciplinaire **HAL**, est destinée au dépôt et à la diffusion de documents scientifiques de niveau recherche, publiés ou non, émanant des établissements d'enseignement et de recherche français ou étrangers, des laboratoires publics ou privés.



Distributed under a Creative Commons Attribution - NonCommercial 4.0 International License



Development, Synthesis, and ^{68}Ga -Labeling of a Lipophilic Complexing Agent for Atherosclerosis PET Imaging

Jennyfer Yong-Sang^{a,b}, Fabienne Dioury^b, Vincent Meneyrol^c, Imade Ait-Arsa^c, Jean-Patrick Idoumbin^c, Florian Guibbal^a, Jessica Patché^a, Fanny Gimié^c, Ilya Khantalina^{a,d}, Joël Couprie^a, Pierre Giraud^a, Sébastien Benard^c, Clotilde Ferroud^b, Emmanuelle Jestin^{a,c}, and Olivier Meilhac^{a,d*}

^(a) Université de La Réunion, Inserm, UMR 1188 Diabète athérombose Thérapies Réunion Océan Indien (DéTROI), Plateforme CYROI, 2 rue Maxime Rivière 97490 Sainte-Clotilde, Réunion France

^(b) Laboratoire de Génomique, Bioinformatique, et Chimie Moléculaire, EA 7528, Conservatoire national des arts et métiers, 2 rue Conté, 75003 Paris, HESAM Université

^(c) Groupe d'Intérêt Public, Cyclotron Réunion Océan Indien, 2 rue Maxime Rivière 97490 Sainte-Clotilde, Réunion, France

^(d) CHU de La Réunion, Allée des Topazes 97400 Saint-Denis, Réunion, France

ARTICLE INFO

Article history:

Received

Revised

Accepted

Available online

Keywords:

Atherosclerosis

Imaging agents

Positron Emission Tomography

HDL

Radiochemistry

ABSTRACT

Cardiovascular disease is the leading cause of mortality and morbidity worldwide. Atherosclerosis accounts for 50% of deaths in western countries. This multifactorial pathology is characterized by the accumulation of lipids and inflammatory cells within the vascular wall, leading to plaque formation. We describe herein the synthesis of a PCTA-based $^{68}\text{Ga}^{3+}$ chelator coupled to a phospholipid biovector 1,2-distearoyl-*sn*-glycero-3-phosphoethanolamine (DSPE), which is the main constituent of the phospholipid moiety of High-Density Lipoprotein (HDL) phospholipid moiety. The resulting ^{68}Ga -PCTA-DSPE inserted into HDL particles was compared to ^{18}F -FDG as a PET agent to visualize atherosclerotic plaques. Our agent markedly accumulated within mouse atheromatous aortas and more interestingly in human endarterectomy carotid samples. These results support the potential use of ^{68}Ga -PCTA-DSPE-HDL for atherosclerosis PET imaging.

2009 Elsevier Ltd. All rights reserved.

1. Introduction

In industrialized countries, atherosclerosis and more particularly its complications including myocardial infarction and ischemic stroke are responsible for about 50% of deaths [1]. The atherosclerotic process is characterized by an accumulation of lipids and inflammatory cells within the wall of medium/large arteries. These depositions can evolve towards the formation of a necrotic core encapsulated by a fibrous cap. These stenosing plaques, particularly rich in lipids, may eventually rupture causing thrombosis, resulting in the obstruction of the vessel and subsequent clinical complications [2]. In this context, more accurate diagnostic methods for early detection of plaque vulnerable to rupture represent an important challenge for medicine. In recent years, much effort has been put to developing non-invasive imaging techniques that would allow assessment of atherosclerotic plaque vulnerability [3]. High-Density Lipoproteins (HDLs) are small endogenous nanoparticles (8-12 nm) involved in cholesterol metabolism and their plasma concentration is negatively correlated to cardiovascular disease. Reverse transport of cholesterol from peripheral tissues back to the liver by HDL particles enables them to reach atherosclerotic

plaques where they take up cholesterol in excess [4]. This property of HDL to transit into lipid-rich plaques and the possibility to *in vitro* chemically modify these particles make them attractive candidates for atherosclerosis imaging [4]. Fayad's group pioneered the use of labeled HDLs for the detection of atheromatous plaques using Magnetic Resonance Imaging (MRI) with Gd(III) and Positron Emission Tomography (PET) with ^{89}Zr ($t_{1/2} = 78.4$ hours) [5-8]. PET high sensitivity permits the use of picomolar concentrations of radiotracers. ^{18}F -fluorodeoxyglucose (^{18}F -FDG) is the most widely used PET tracer in clinical practice, mainly for tumor detection. However, it lacks specificity for targeting atherosclerosis due to the heterogeneity of glucose consumption by vascular and inflammatory cells [9]. Gallium has been used in a large spectrum of applications including detection of tumors, infectious processes or atherosclerosis, using either ^{67}Ga ($t_{1/2} = 78$ hours) for Single Photon Emission Computed Tomography (SPECT) or $^{68}\text{Ga}^{3+}$ ($t_{1/2} = 68$ minutes) for PET imaging [10,11]. $^{68}\text{Ga}^{3+}$ can be conveniently produced by a $^{68}\text{Ge}/^{68}\text{Ga}$ generator, eliminating the need for considerably more expensive cyclotrons, and its short half-life is compatible with clinical diagnosis applications. One of the main limitations

encountered for *in vivo* $^{68}\text{Ga}^{3+}$ administration is the need of a well-chosen ligand associated with a strong coordination in order to prevent metallic ion release [12,13]. The use of acyclic chelating agents such as DFO (desferrioxamine mesylate), EDTA (ethylenediamine tetraacetic acid) and DTPA (diethylenetriaminepentaacetic acid) results in transchelation with apotransferrin [13]. Thus, these agents were supplanted by macrocyclic structures such as DOTA and NOTA (respectively 1,4,7,10-tetraazacyclododecane-1,4,7,10-tetraacetic and 1,4,7-triazacyclononane-1,4,7-trisacetic acids), due to their superior kinetic inertness and thermodynamic stability (Fig. 1). NOTA (N_3O_3 chelator), is currently the first choice for $^{67/68}\text{Ga}(\text{III})$ -based medical imaging agents (mild labeling conditions, stable complexation). N_4O_4 chelating agents such as DOTA are also used for SPECT/PET with $\text{Gd}(\text{III})$ for MRI applications in spite of their limited ability to chelate $^{67/68}\text{Ga}(\text{III})$ [11,14]. Recent investigations showed that the N_4O_3 12-membered macrocyclic-chelating agent PCTA (pentadeca-1(15),11,13-triene-3,6,9-triacetic acid) (Fig. 1), with intermediate denticity between NOTA and DOTA, was more suitable than DOTA for ^{68}Ga -labeling. It exhibits much faster kinetics at room temperature, together with the superior stability of the Ga-PCTA complex in serum [10]. PCTA, a rigidified DOTA analog bearing a pyridine, allows very stable coordination either with $\text{Gd}(\text{III})$ or $\text{Ga}(\text{III})$ in comparison with other chelates [15-17].

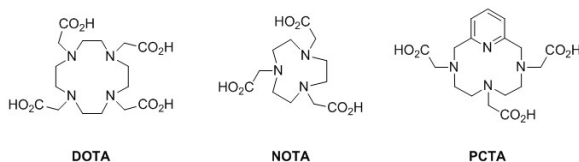


Fig. 1 Chemical structures of DOTA, NOTA, and PCTA.

We have previously reported the synthesis of the 3-pyridinol-based compound **3** as a precursor of an amphiphilic PCTA chelating agent for MRI application [18]. We describe herein an optimized overall experimental procedure leading to the functionalizable prochelator **4**. This compound bears a pyridine subunit with an additional carboxylic acid function allowing conjugation with DSPE (1,2-distearoyl-*sn*-glycero-3-phosphoethanolamine). Similarly to our reported synthetic route [18], the dodecylamine was replaced by DSPE, a phospholipid naturally present in the HDL lipid layer, which allows PCTA-DSPE insertion into these particles (Fig. 2). In order to radiolabel HDLs with $\text{Ga}(\text{III})$, two approaches were considered: either by mixing PCTA-DSPE chelating agent with HDL particles, followed by addition of $^{68}\text{Ga}(\text{III})$ or by introducing the $^{68}\text{Ga}(\text{III})$ -PCTA-DSPE into the HDL lipid layer. The second strategy was chosen to avoid potential HDL denaturation.

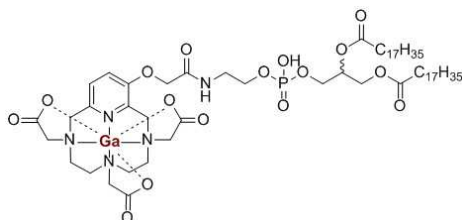
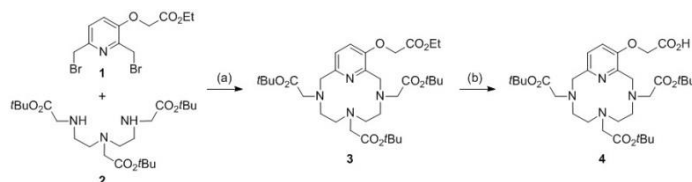


Fig. 2 PCTA-DSPE radiolabeled with $^{68}\text{Ga}(\text{III})$.

2. Results and discussion

The PCTA derivative **3** was obtained as described previously [18] with optimized protocols to prepare starting materials **1** and **2** (see supporting information S2 and S3). The macroring

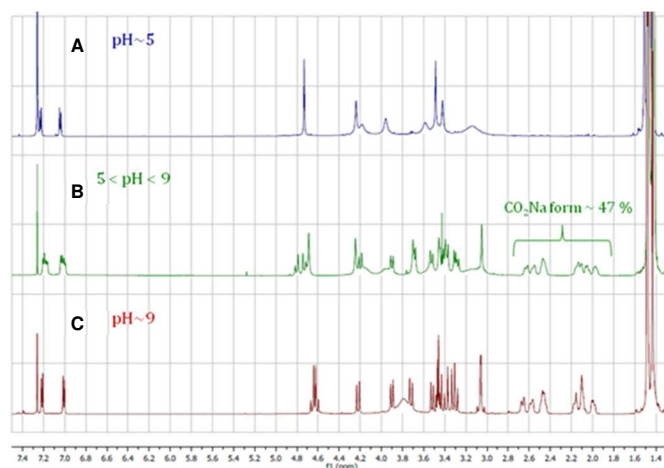
formation was carried out at room temperature in a less diluted medium compared to Picard's procedure [19]; in such conditions, the macrocycle **3** was isolated with a 76% yield. A selective deprotection of the ethyl ester was achieved by controlled saponification with NaOH in an aqueous ethanolic medium leading to the basic carboxylate. After treatment with a stoichiometric amount of hydrochloric acid, the targeted prochelator **4** was obtained with a 63% yield over the two steps (Scheme 1).



Scheme 1. Synthesis of prochelator **4**. Reagents and conditions: (a) Na_2CO_3 , DMF, rt, 24h; (b) i) NaOH_{aq} , EtOH, rt, 1h; ii) HCl_{aq} , 63% (2 steps).

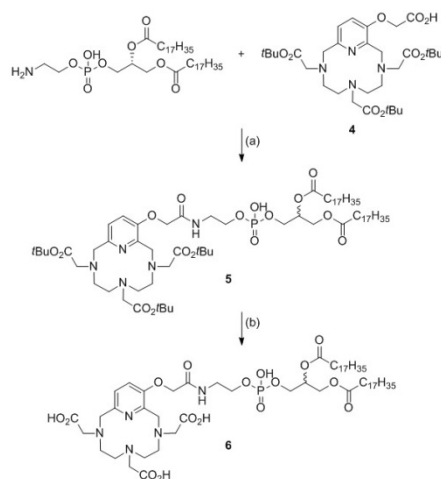
It is noteworthy that the final acidification step induced a strong line-broadening of CH_2 resonances in the region 2-5 ppm (Fig. 3A) that can be rationalized by the formation of a zwitterion species with several forms in equilibrium at the NMR timescale. NMR characterization was thus preferred before acidic treatment at $\text{pH} \sim 9$ to maintain the CO_2Na form (Fig. 3C). A mixture of the two forms was obtained if $5 < \text{pH} < 9$ (Fig. 3B).

Fig. 3 pH dependence of **4** ^1H -NMR spectra (CDCl_3) showing CO_2H form at $\text{pH} \sim 5$ (A), CO_2Na form at $\text{pH} \sim 9$ (C) and a mixture of the two forms at pH



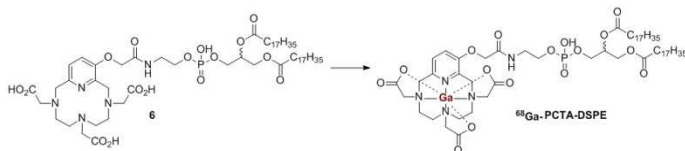
ranged between 5 and 9 (B).

Conjugation to DSPE was achieved with compound **4** in its CO_2H form since Na^+ may interfere with PCTA chelation [19]. On the basis of Nicolay's work on DOTA-tris(*t*Bu) [14], it occurred by activation with TSTU (*N,N,N',N'*-Tetramethyl-*O*-(*N*-succinimidyl)uronium tetrafluoroborate) in the presence of DIPEA (*N,N*-diisopropylethylamine) in a mixture of DMF (*N,N*-dimethylformamide)/ CHCl_3 , and led to compound **5** with a 72% yield. The final step consisted of complete *tert*-butyl ester cleavage by repeated treatments with TFA (Trifluoroacetic acid), leading to PCTA-DSPE **6** with a 67% yield (Scheme 2). The product was characterized by NMR, HRMS and HPLC-MS. The natural ability of DSPE to self-assemble into micelles was investigated by Dynamic Light Scattering (DLS). Two populations of nanoparticles were observed: 39 and 293 nm (see supporting information, Fig. S8).



Scheme 2. DSPE coupling. Reagents and conditions: (a) TSTU, DiPEA, DMF, rt, 1h, then DSPE, DIPEA, CHCl₃, 65°C, 3h, 72%; (b) TFA/CHCl₃ 3/7 (v/v), 72%.

PCTA-DSPE **6** radiolabeling was performed with ⁶⁸GaCl₃ produced by a ⁶⁸Ge/⁶⁸Ga generator (Galli Eo™, IRE-Elit, Belgium) without the need of eluate pre-purification (**Scheme 3**). This generator affords a fully integrated system for ⁶⁸GaCl₃ elution with 0.1 M HCl. The high purity of the eluate in a small volume (1.1 mL) is suitable for a one-pot radiolabeling step with the chelating agent in the reactor without compromising the radiochemical yield and purity. 2 mg of compound **6** were dissolved at 80°C in 0.2 M NaOAc buffer (pH = 5). The precursor **6** was incubated with 1.1 mL of eluate for 10 min at 80°C (resulting pH = 4).



Scheme 3. PCTA-DSPE **6** radiolabeling with ⁶⁸GaCl₃.

A PD-10 desalting column was used to remove unreacted ⁶⁸GaCl₃ and to elute the radiolabeled ⁶⁸Ga-PCTA-DSPE in PBS (pH = 7.4) before insertion into HDLs. ⁶⁸Ga-PCTA-DSPE was finally obtained with a decay-corrected radiochemical yield (RCY) of 70% and a high radiochemical purity > 99% (**Fig. 4**).

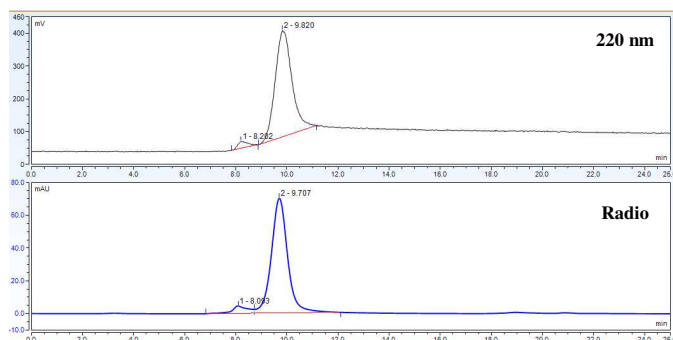


Fig. 4 UV/radio-HPLC profiles of ⁶⁸Ga-PCTA-DSPE (Superdex Increase 200 10/300 GL – PBS 1X, pH 7.4 flow rate of 1 mL/min)

HDLs were isolated from human serum following a previously reported procedure [20]. Radiolabeled micelles of ⁶⁸Ga-PCTA-DSPE were incubated with 1 mL HDL solution (10 mg/mL of proteins) at 37°C for 15 min. The complete insertion of the radiolabeled micelles was assessed by HPLC. Radiolabeled HDLs, ⁶⁸Ga-PCTA-DSPE-HDL (later abbreviated " ⁶⁸Ga-HDL"), were obtained with radiochemical purity of over 98% (**Fig. 5**), suitable for preclinical studies. ⁶⁸Ga-HDL stability was evaluated in phosphate buffer and human serum at 30, 60 and 90 min with less than 5% of degradation observed (see **supporting information Fig. S1, S2, S3, S4 and S5**).

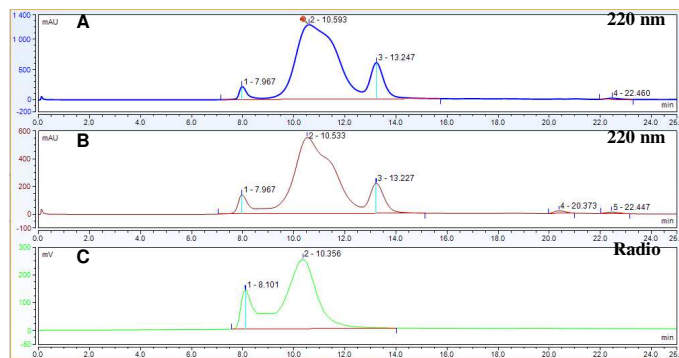


Fig. 5 UV/radio-HPLC profiles of unlabeled HDL (A) and ⁶⁸Ga-HDL (B/C). (Superdex Increase 200 10/300 GL – PBS 1X, pH 7.4 flow rate of 1 mL/min)

In order to test the ability of ⁶⁸Ga-HDL to image atherosclerosis, it was injected into a mouse model known to develop aortic atheroma (ApoE deficient mice, ApoE KO). Our radiotracer was compared to the well-established ¹⁸F-FDG expected to accumulate in glucose-consuming inflammatory cells associated with atherosclerotic plaques [9]. The biodistribution of ⁶⁸Ga-HDL was also compared to that of ⁶⁸Ga-PCTA-DSPE in order to demonstrate the specificity of HDLs for targeting atheromatous plaques. ⁶⁸Ga-PCTA-DSPE, ⁶⁸Ga-HDL or ¹⁸F-FDG (15 ± 5 MBq) were injected *via* the caudal vein in 10 months-old ApoE KO mice. This animal model allowed us to test the ability of ⁶⁸Ga-HDL to image atheromatous plaques. Taking advantage of HDL reverse transport of cholesterol from the plaque back to the liver, we were able to show that these particles accumulate sufficiently within atheromatous plaques to be used as radioactive probes for PET imaging, as also reported by other groups [5].

As depicted in **Fig. 6**, whole body imaging was performed at 30 min. In ApoE KO mice, no significant positive signal was observed in the vascular system regardless of the radiotracer used. This may be due to the high uptake by other organ such as liver (23 ± 6 and 23 ± 4 %ID/g) and heart (12 ± 2 and 11 ± 1 %ID/g) respectively for ⁶⁸Ga-PCTA-DSPE and ⁶⁸Ga-HDL, respectively, which potentially masks the aortic signal, since the aorta follows the course of the spine. Injection in C57BL/6 wild type mice gave similar results with accumulation in the liver (31 ± 4 and 29 ± 4 %ID/g) and the heart (22 ± 2 and 19 ± 4 %ID/g) respectively for ⁶⁸Ga-PCTA-DSPE and ⁶⁸Ga-HDL (see **supporting information, Fig. S6**).

⁶⁸Ga-PCTA-DSPE and ⁶⁸Ga-HDL accumulated mainly in the liver, in accordance with HDL metabolism and nanomicelles catabolism [4,21]. Liver is the keystone of lipid metabolism, in particular for lipoproteins, which are taken up from the blood stream using specific receptors such as SRB1 (scavenger receptor type 1) for HDLs. In comparison, ¹⁸F-FDG accumulated in glucose-consuming organs (brain and heart) whereas kidneys and bladder also showed a high signal, as they are involved in glucose elimination.

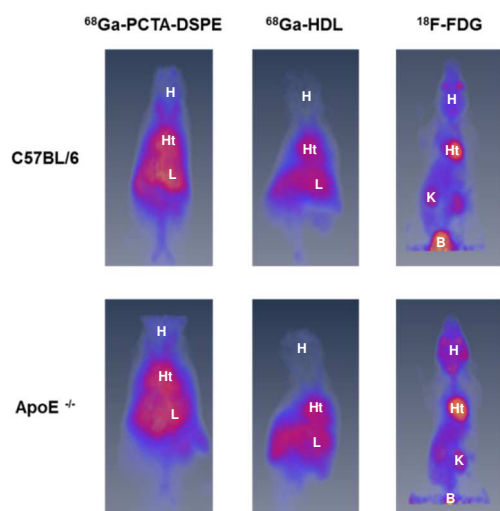


Fig. 6 Whole body PET images of C57BL/6 control (top row) and ApoE KO (bottom row) mice. From left to right: ^{68}Ga -PCTA-DSPE, ^{68}Ga -HDL and ^{18}F -FDG radiotracers; B (Bladder), H (Head), Ht (Heart), K (Kidneys), L (Liver).

In order to evaluate the potential accumulation of ^{68}Ga -PCTA-DSPE and ^{68}Ga -HDL within atheromatous vessels, the heart and the aorta were dissected out 30 min post-injection and imaged *ex vivo* (15 min PET acquisition). The aortas were then opened longitudinally, split and pinned onto a black wax surface, to expose the atheromatous plaques. Macroscopic photographs of plaques were compared to *ex vivo* PET images (Fig. 7). As depicted in Fig. 7, no signal was detected in the aorta of C57BL/6 control mice injected with ^{68}Ga -PCTA-DSPE, ^{68}Ga -HDL or ^{18}F -FDG. However, a strong positivity in different areas of the aorta was observed in ApoE KO mice injected with ^{68}Ga -HDL, correlating with the presence of atheromatous plaques as shown on macroscopic views while no positive signal was observed with either ^{68}Ga -PCTA-DSPE or ^{18}F -FDG. As a result, ^{68}Ga -HDL could represent a good radiotracer for detection of atheromatous lipid-rich plaques.

Accumulation of HDL particles within atheromatous plaques of injected mice was also confirmed by immunohistofluorescence (see supporting information, Fig. S9)

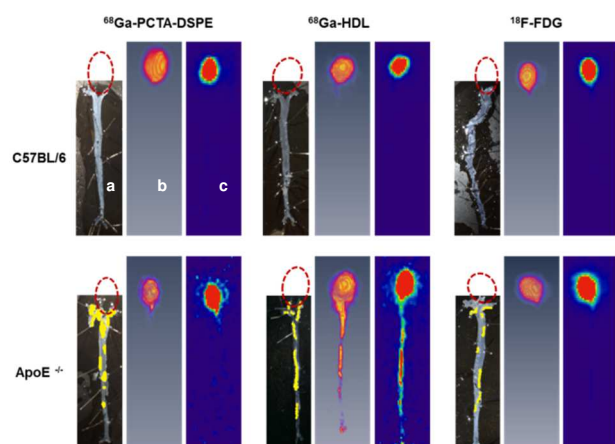


Fig. 7 Images of aorta and heart of C57BL/6 control (top panel) and ApoE KO (bottom panel) mice. From left to right, ^{68}Ga -PCTA-DSPE, ^{68}Ga -HDL

and ^{18}F -FDG radiotracers: (a) Macroscopic view; (b) 3D PET image; (c) 2D PET image. The heart was removed before dissection of the aorta; its position is indicated with a red dashed circle. Atheromatous plaques have been highlighted in yellow.

In order to strengthen these results, we evaluated the ability of ^{68}Ga -HDL to label human carotid atherosclerotic samples characterized by both non-complicated lipid-rich plaques and more advanced complicated lesions containing intraplaque hemorrhages. Both ^{68}Ga -HDL and ^{18}F -FDG were tested *ex vivo* in freshly obtained carotid endarterectomy samples. As shown in Fig. 8, ^{18}F -FDG-incubated carotid samples displayed a strong signal only in the stenosed complicated plaque sample. More interestingly, ^{68}Ga -HDL particles were able to accumulate in both complicated and non-complicated parts of atherosclerotic carotid samples. This underlines the greater ability of our radiotracer to accumulate within lipid-rich plaques that are prone to rupture even in non-stenosing conditions.

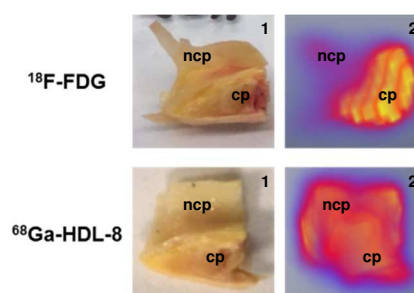


Fig. 8 *Ex vivo* accumulation of ^{68}Ga -HDL (bottom panels) and ^{18}F -FDG (top panels) radiotracers in human carotid endarterectomy samples: macroscopic view (left), and 3D PET images (right); ncp: non-complicated plaque, cp: culprit plaque corresponding to the stenosed part of the same carotid sample.

3. Conclusion

We have synthesized for the first time a PCTA-derivative chelate coupled with DSPE. Our chelating agent was able to efficiently coordinate $^{68}\text{Ga}^{3+}$ with a 70% RCY. Finally, our radiotracer was completely inserted into the HDL lipid layer. Atherosclerosis PET imaging performed in both a murine model and human *ex vivo* samples showed a better potential of our tracer than ^{18}F -FDG whose accumulation was limited to metabolically active cells. These preliminary results have demonstrated that our new lipid-based agent able to chelate a short half-life isotope (^{68}Ga , $t_{1/2} = 68$ min) could be used for diagnosis of atherosclerosis. Formulation of ^{68}Ga -PCTA-DSPE with synthetic HDL particles injectable into human or other nanomicelles could allow a wider use in different clinical settings [22].

Acknowledgments

This work was supported by European Regional Development Funds RE0007810 and RE0001897 (EU- Région Réunion - French State national counterpart). and JYS was funded by a doctoral grant from Région Réunion n°181695, Fondation pour la Recherche Médicale n°FDT20160435551 and a postdoctoral fellowship from Fondation de France. The authors would like to thank the Radiopharmaceutical Production Service for supplying ^{18}F -FDG. We thank Dr. Mary Osborne-Pellegrin for help in editing the manuscript.

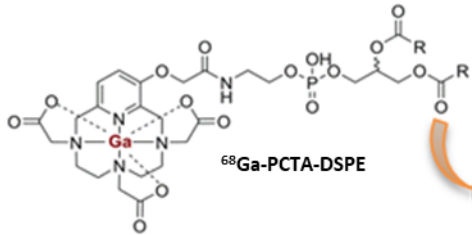
Supplementary Material

Supplementary data related to this article can be found at XXX.

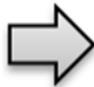
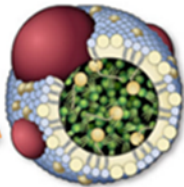
References and notes

There are no conflicts to declare. **All authors have contributed to writing the manuscript and** have given approval to the final version of the manuscript.

- [1] WHO, Fact sheet #317, (2012).
- [2] A.J. Lusis, *Atherosclerosis*, *Nature*, 407 (2000) 233-241.
- [3] Y. Shimizu, Y. Kuge, Recent Advances in the Development of PET/SPECT Probes for Atherosclerosis Imaging, *Nucl. Med. Mol. Imaging*, 50 (2016) 284-291.
- [4] R. Kuai, D. Li, Y.E. Chen, J.J. Moon, A. Schwendeman, High-Density Lipoproteins: Nature's Multifunctional Nanoparticles, *ACS Nano*, 10 (2016) 3015-3041.
- [5] C. Perez-Medina, T. Binderup, M.E. Lobatto, J. Tang, C. Calcagno, L. Giesen, C.H. Wessel, J. Witjes, S. Ishino, S. Baxter, Y. Zhao, S. Ramachandran, M. Eldib, B.L. Sanchez-Gaytan, P.M. Robson, J. Bini, J.F. Granada, K.M. Fish, E.S. Stroes, R. Duivenvoorden, S. Tsimikas, J.S. Lewis, T. Reiner, V. Fuster, A. Kjaer, E.A. Fisher, Z.A. Fayad, W.J. Mulder, *In Vivo PET Imaging of HDL in Multiple Atherosclerosis Models*, *JACC Cardiovasc. Imaging*, 9 (2016) 950-961.
- [6] D.P. Cormode, J.C. Frias, Y. Ma, W. Chen, T. Skajaa, K. Briley-Saebo, A. Barazza, K.J. Williams, W.J.M. Mulder, Z.A. Fayad, E.A. Fisher, HDL as a contrast agent for medical imaging, *Clin. Lipidol.* 4 (2009) 493-500.
- [7] D.P. Cormode, K.C. Briley-Saebo, W.J. Mulder, J.G. Aguinaldo, A. Barazza, Y. Ma, E.A. Fisher, Z.A. Fayad, An ApoA-I mimetic peptide high-density-lipoprotein-based MRI contrast agent for atherosclerotic plaque composition detection, *Small*, 4 (2008) 1437-1444.
- [8] D.P. Cormode, R. Chandrasekar, A. Delshad, K.C. Briley-Saebo, C. Calcagno, A. Barazza, W.J.M. Mulder, E.A. Fisher, Z.A. Fayad, Comparison of Synthetic High Density Lipoprotein (HDL) Contrast Agents for MR Imaging of Atherosclerosis, *Bioconjug. Chem.* 20 (2009) 937-943.
- [9] J.H.F. Rudd, E.A. Warburton, T.D. Fryer, H.A. Jones, J.C. Clark, N. Antoun, P. Johnström, A.P. Davenport, P.J. Kirkpatrick, B.N. Arch, J.D. Pickard, P.L. Weissberg, Imaging Atherosclerotic Plaque Inflammation With [¹⁸F]-Fluorodeoxyglucose Positron Emission Tomography, *Circulation*, 105 (2002) 2708-2711.
- [10] C.L. Ferreira, E. Lamsa, M. Woods, Y. Duan, P. Fernando, C. Bensimon, M. Kordos, K. Guenther, P. Jurek, G.E. Kiefer, Evaluation of bifunctional chelates for the development of gallium-based radiopharmaceuticals, *Bioconjug. Chem.* 21 (2010) 531-536.
- [11] E. Blom, J. Kozirowski, ⁶⁸Ga-autoclabeling of DOTA-TATE and DOTA-NOC, *Int. J. Appl. Radiat. Is.* 70 (2012) 980-983.
- [12] L. Lattuada, A. Barge, G. Cravotto, G.B. Giovenzana, L. Tei, The synthesis and application of polyamino polycarboxylic bifunctional chelating agents, *Chem. Soc. Rev.* 40 (2011) 3019-3049.
- [13] P. Spang, C. Herrmann, F. Roesch, Bifunctional Gallium-68 Chelators: Past, Present, and Future, *Semin. Nucl. Med.* 46 (2016) 373-394.
- [14] S. Hak, H.M. Sanders, P. Agrawal, S. Langereis, H. Grull, H.M. Keizer, F. Arena, E. Terreno, G.J. Strijkers, K. Nicolay, A high relaxivity Gd(III)DOTA-DSPE-based liposomal contrast agent for magnetic resonance imaging, *Eur. J. Pharm. Biopharm.* 72 (2009) 397-404.
- [15] F. Dioury, E. Guéné, A.D. Scala-Rouilleau, C. Ferroud, A. Guy, M. Port, Synthesis of a new tricyclic tetraazatriacetic acid as ligand for gadolinium(III), *Tetrahedron Lett.* 46 (2005) 611-613.
- [16] C.L. Ferreira, D.T. Yapp, D. Mandel, R.K. Gill, E. Boros, M.Q. Wong, P. Jurek, G.E. Kiefer, ⁶⁸Ga small peptide imaging: comparison of NOTA and PCTA, *Bioconjug. Chem.* 23 (2012) 2239-2246.
- [17] R. Chakravarty, R. Shukla, R. Ram, A.K. Tyagi, A. Dash, M. Venkatesh, Development of a nano-zirconia based ⁶⁸Ge/⁶⁸Ga generator for biomedical applications, *Nucl. Med. Biol.* 38 (2011) 575-583.
- [18] C. Ferroud, H. Borderies, E. Lasri, A. Guy, M. Port, Synthesis of a novel amphiphilic GdPCTA-[12] derivative as a potential micellar MRI contrast agent, *Tetrahedron Lett.* 49 (2008) 5972-5975.
- [19] M. Enel, N. Leygue, N. Saffon, C. Galaup, C. Picard, Facile Access to the 12-Membered Macrocyclic Ligand PCTA and Its Derivatives with Carboxylate, Amide, and Phosphinate Ligating Functionalities, *Eur. J. Org. Chem.* 2018 (2018) 1765-1773.
- [20] G. Ortiz-Muñoz, X. Houard, J.-L. Martín-Ventura, B.Y. Ishida, S. Loyau, P. Rossignol, J.-A. Moreno, J.P. Kane, R.J. Chalkley, A.L. Burlingame, J.-B. Michel, O. Meilhac, HDL antielastase activity prevents smooth muscle cell anoikis, a potential new antiatherogenic property, *FASEB J.* 23 (2009) 3129-3139.
- [21] M. Bartneck, K.T. Warzecha, F. Tacke, Therapeutic targeting of liver inflammation and fibrosis by nanomedicine, *Hepatobiliary Surg. Nutr.*, 3 (2014) 364-376.
- [22] P. Tricoci, D.M. D'Andrea, P.A. Gurbel, Z. Yao, M. Cuchel, B. Winston, R. Schott, R. Weiss, M.A. Blazing, L. Cannon, A. Bailey, D.J. Angiolillo, A. Gille, C.L. Shear, S.D. Wright, J.H. Alexander, Infusion of Reconstituted High-Density Lipoprotein, CSL112, in Patients With Atherosclerosis: Safety and Pharmacokinetic Results From a Phase 2a Randomized Clinical Trial, *J. Am. Heart Assoc.* 4 (2015) e002171.



HDL



ApoE KO



Mouse aortas

